Spectroscopic characterization of exoplanets : from LOUPE to SINFONI

Hoeijmakers, H.J.

5

MEDIUM-RESOLUTION INTEGRAL-FIELD SPECTROSCOPY FOR HIGH-CONTRAST EXOPLANET IMAGING: MOLECULE MAPS OF THE β PICTORIS SYSTEM WITH SINFONI

Angular Differential Imaging (ADI) and Spectral Differential Imaging (SDI) are well-established high-contrast imaging techniques but their application is challenging for companions at small angular separations from their host stars. The aim of this study is to investigate to what extent adaptive-optics assisted, medium-resolution ($R \sim 5000$) integral field spectrographs (IFS) can be used to directly detect the absorption of molecular species in the spectra of planets and substellar companions, which are not present in the spectrum of the star. We analysed archival data of the β Pictoris system taken with the SINFONI integral field spectrograph located at ESO's Very Large Telescope, originally taken to image β Pictoris b using ADI techniques. At each spatial position in the IFS, a scaled version of the stellar spectrum is subtracted from the data after which the residuals are cross-correlated with model spectra. The cross-correlation co-adds the individual absorption lines of the planet emission spectrum constructively, while this is not the case for (residual) telluric and stellar features. Cross-correlation with CO and H_2O models result in significant detections of β Pictoris b at 6.9σ and 11.0σ respectively, at an angular distance of 0.36" from the star. Correlation with a $T = 1700$K BT-Settl model provides a 14.4σ detection. This in contrast to data analysis using the LOCI (ADI) algorithm which barely reveals the planet. While the adaptive optics system only achieved modest Strehl ratios of 19-27% and a raw contrast of 1:300 at the planet position, cross-correlation achieves a 3σ contrast limit of 4.4×10^{-5} in this 2.5 hr data set. Adaptive-optics assisted, medium-resolution IFS such as SINFONI on the VLT and OSIRIS on the Keck Telescope, can be used for high-contrast imaging utilizing cross-correlation techniques for planets that are close to their star and embedded in speckle noise. We refer to this method as "molecule mapping" and advocate its application to observations with future medium resolution instruments, in particular HARMONI on the ELT and NIRSpec and MIRI on the JWST.

Hoeijmakers, Schwarz, Snellen et al.
To be submitted.

5.1 INTRODUCTION

To directly image an extrasolar planet, the light of its host star must generally be suppressed by orders of magnitude. The techniques that have been developed to do this rely on a combination of precise wave front control (adaptive optics), possible smoothing of the diffraction pattern of the telescope (pupil apodization), blocking the star with a mask (coronography) and/or by using interferometric optics to make the starlight interfere destructively with itself (phase masks). In such imaging data, residual starlight is present in the form of speckles which may mimic point-source objects, confusing the detection of companions and planets. Such residuals can be suppressed during post-processing by assuming that the pattern is fixed to the orientation of the telescope (angular differential imaging, ADI), that such a pattern scales with wavelength (spectral differential imaging, SDI), and/or by modelling the time-variability of the speckles (e.g. principal component analysis, PCA) (see e.g. Guyon, 2011; Mawet et al., 2012; Chauvin, 2016, for reviews).

So far, direct imaging detections are generally limited to a specific part of the exoplanet population: Young gas giants in wide orbits that glow by radiating out the internal heat that resulted from their formation. These planets can be resolved from their host star owing to their relatively large mutual angular separation and the fact that they are self-luminous at infrared wavelengths. Such planets can generally only be observed during the first few tens of millions of years of their lifetime, after which they have cooled too much to be detected with current facilities (see e.g. Bowler, 2016, for a review).

The desire to image cooler (i.e. older or less massive) planets that are closer to their host star is fuelling the development of new instruments, and observing and data analysis techniques. The arsenal of high-contrast imaging facilities has recently been expanded by the deployment of dedicated planet finding instruments such as the Gemini Planet Finder (Macintosh et al., 2006) at the Gemini Telescope, SPHERE (Beuzit et al., 2008) on the European Very Large Telescope (VLT), and SCExAO (Jovanovic et al., 2015) on the Subaru telescope. These instruments also have low-resolution ($R \sim 30 - 100$) spectroscopic capability - allowing the spectal characterization of directly imaged planets, achieving planet-to-star contrast ratios down to 10^{-6} at 0.2" angular separation (see e.g. Macintosh et al., 2014; Ruffio et al., 2017; Mesa et al., 2017; Currie et al., 2017).

5.1.1 *Integral field spectroscopy*

Multiple studies indicate that when high-contrast imaging is combined with high-dispersion spectroscopic techniques, the achieved contrasts can be significantly enhanced (see e.g. Sparks et al., 2002; Riaud et al., 2007; Kawahara

et al., 2014; Snellen et al., 2015; Luger et al., 2017; Wang et al., 2017). Such strategies assume that the faint planet and the much brighter star have spectral properties that are distinctly different at high spectral resolution; notably the presence of molecular absorption bands in the spectrum of the planet. Because the planet is close to the star, its spectrum is deeply embedded in speckle-noise, but it can be extracted using cross-correlation: The cross-correlation co-adds the individual absorption lines of the planet constructively, but not stellar and telluric features, or at a different radial velocity. This method has been applied successfully for the first time by Snellen et al. (2014) at high spectral resolution, albeit using the CRIRES slit spectrograph that probes only one spatial dimension. This resulted in the measurement of the spin of β Pictoris b (Snellen et al., 2014).

In this study we investigate to what extent this method can be applied to data from adaptive-optics assisted, medium-resolution ($R \sim 5000$) integral field spectrographs (IFS) - targeting molecular species in a planet atmosphere that are not present in the star throughout the two-dimensional field of view. The use of cross-correlation techniques on IFS data was first performed by Konopacky et al. (2013) and Barman et al. (2015) to detect H_2O, CO and CH_4 in the atmospheres of HR 8799 b&c using the OSIRIS integral field spectrograph at the Keck Observatory. At 1.7" and 0.96", HR 8799 b&c are widely separated from their host star (Marois et al., 2008). Such angular distances are well resolvable by modern adaptive-optics systems and the speckle-pattern can be effectively removed using ADI or SDI-based methods. However, the application of ADI and SDI are less effective at smaller angular separations because the effects of field rotation and wavelength-dependencies are limited (Fitzgerald et al., 2006; Lafrenière et al., 2007; Marois et al., 2008; Rameau et al., 2015).

We apply the cross-correlation technique to archival K-band SINFONI image cubes of the β Pictoris system and are able to extract the spectral signature of the planet β Pictoris b, while effectively removing the diffraction pattern of the star in which the planet is embedded. We refer to this technique as *molecule mapping* because it produces two-dimensional cross-correlation maps that show where in the image certain molecules are detected.

In Section 5.2 we describe the β Pictoris system. Section 5.3 describes the archival SINFONI observations used in this analysis and the data reduction. The cross-correlation procedure is described in Section 5.4, followed by the resulting cross-correlation images in Section 5.5, including a comparison with the LOCI algorithm (Lafrenière et al., 2007). Paragraphs 5.5.4 and 5.5.5 highlight potential application of molecule mapping with upcoming medium-resolution integral-field instruments on the ELT and JWST, after which the paper is summarized and concluded in Section 5.6.

5.2 THE β PICTORIS SYSTEM

In 1984, β Pictoris was the first star to be found to host a debris disk, associated with planet formation processes (Smith et al., 1984). The warped structure of the disk led to the inference of a possible planetary mass companion (Scholl et al., 1993; Roques et al., 1994; Lazzaro et al., 1994; Burrows et al., 1995; Lecavelier des Etangs et al., 1996; Mouillet et al., 1997; Augereau et al., 2001), which was discovered in 2008 (Lagrange et al., 2009; Lagrange et al., 2010) via direct imaging. The system is a member of the nearby β Pictoris moving group which has an estimated age of 24 ± 3 Myr (Bell et al., 2015). A recent estimate of the bolometric luminosity and effective temperature of the planet by Chilcote et al. (2017) of $\log\left(\frac{L_p}{L_\odot}\right) = -3.78 \pm 0.03$ and 1724 ± 15K respectively, provides a mass of $12.9 \pm 0.2 M_J$ and a radius of $1.46 \pm 0.01 R_J$ (see Table 5.1), assuming a hot-start evolution model (Baraffe et al., 2003).

β Pic b moves on a 20–26-year orbit that is highly inclined with respect to the line of sight from Earth (Wang et al., 2016). This high inclination has recently triggered a renewed interest in this system because the Hill sphere of the planet is predicted to transit the star between April 2017 and January 2018 (Lecavelier des Etangs et al., 2016; Wang et al., 2016; Kenworthy, 2017). Snellen et al. (2014) measured the projected equatorial rotation velocity of the planet, inferring a length of day of ~8 hours.

5.3 OBSERVATIONS

The β Pictoris system was observed with the SINFONI IFS (Eisenhauer et al., 2003) mounted on ESO's the Very Large Telescope in K-band on the nights of September 10 and 11, 2014 as part of ESO programme 093.C-0626(A) (P.I.: Chauvin). The observations on both nights were taken in pupil tracking mode which makes the field rotate during the observing sequence, facilitating Angular Differential Imaging. The 32x64 pixel images were taken in the highest spatial resolution mode, with each pixel covering 0.0125" by 0.025", providing a field of view (FOV) of 0.8" by 0.8" on sky. At a resolving power of $R \sim 5000$ the SINFONI spectra have a wavelength coverage from 1.929 μm to 2.472 μm with a sampling of 0.25 nm. At the time of these observations the planet was separated from the central star by approximately 0.36" (Wang et al., 2016). On the first and second night, 24 and 30 science frames were obtained respectively, spanning a total duration of 2.5 hours (see Table 5.2). During both nights, the seeing varied between 0.7" to 0.9" and the AO system delivered modest Strehl ratios between 19% and 27%. The observations on the first night were preceded by a few acquisition images after which the star was placed just outside the FOV for the rest of the sequence. During the second night both star and planet were observed continuously (see Fig. 5.1).

Parameter	Symbol	Value
Visible magnitude[a]	V	3.86
K-band magnitude[a]	K	3.48
Distance (pc)[b]	d	19.44 ± 0.05
Effective temperature (K)[c]	$T_{\rm eff}$	8052 ± 30
Mass ($M_\odot$)[d]	M_*	$1.85^{+0.03}_{-0.04}$
Metallicity (dex)[c]	[M/H]	0.05 ± 0.06
Age (Myr)[e]		24 ± 3
Rotation velocity (km s^{-1})[f]	$v \sin i$	130
Systemic velocity (km s^{-1})[g]	v	20.0 ± 0.7
Luminosity $\left(\log \frac{L}{L_\odot}\right)$[h]	L_p	-3.78 ± 0.03
K-band contrast[i]	ΔK	9.2 ± 0.1
Effective temperature (K)[h]	$T_{\rm eff}$	1724 ± 15
Surface gravity ($\log g$)[h]		4.18 ± 0.01
Angular separation (mas)[i]		356.5 ± 0.9
Position angle (deg)[j]		213.0 ± 0.2

Table 5.1: Summary of the properties of the star β Pictoris (upper part) and its planet (lower part).
a: Ducati (2002).
b: van Leeuwen (2007).
c: Gray et al. (2006).
d: Wang et al. (2016). The stellar mass was inferred from their fit to the total mass of the system minus the mass of the planet. Although the quoted confidence intervals correspond to 1σ uncertainties, the posterior distributions are non-Gaussian.
e: Bell et al. (2015).
f: Royer et al. (2007).
g: Gontcharov (2006).
h: Chilcote et al. (2017). These authors measured the luminosity from their GPI datasets, but inferred the other parameters using a hot-start evolutionary model by Baraffe et al. (2003). The reported statistical errors do not account for the model-dependency of these values.
i: Bonnefoy et al. (2011).
j: Measurements obtained by Wang et al. (2016) on November 8, 2014.

Observing night	Sept. 10, 2014	Sept. 11, 2014
N_{exp}	24	30
DIT (s)	60	2
NDIT	4	50
Airmass	1.34 - 1.15	1.49 - 1.14
PA (deg)	340.7 - 304.6	355.7 - 304.3
Strehl ratio (%)	19 - 27	20 - 25

Table 5.2: Overview of the observations of the the β Pictoris system of September 10 and 11, 2014, showing the number of exposures N_{exp}, the exposure time per dithering position (DIT), the number of dithering positions combined to make each science frame (NDIT), and the range of airmasses, position angles on sky, and approximate Strehl ratios achieved.

The raw data was downloaded from the ESO Science Archive Facility and reduced using version 3.0.0 of the SINFONI pipeline. The reduction pipeline produces a three-dimensional image cube for each science observation, with sky position in the x and y directions and wavelength in the z direction. The pipeline reduced data cubes contain NAN values at the edges of the waveband and at the location of known bad pixels. To reject these areas, we only consider wavelengths between 2.088 μm and 2.452 μm and flag any remaining NAN values (see Figure 5.2). From each science exposure we obtain the wavelength-averaged two-dimensional image. The spatial location of the star was found by fitting a two-dimensional Gaussian profile to a region of 10×10 pixels around the maximum of the PSF. We use this location as a pivot to derotate all image-cubes by their respective position angle and to align them to a common frame. We co-added all image cubes of each night to obtain two master image cubes, excluding all regions within a range of 5 pixels from the edges of the individual frames. The wavelength-averaged images of these two master cubes are shown in Figure 5.1. From the wavelength-averaged image of the second night, we constructed a curve of the raw contrast as a function of angular separation from the star, and measure the raw contrast at the separation of the planet to be 1:300 (see Figure 5.8).

We subsequently applied our cross-correlation analysis to the master cubes of both nights independently as described in the next section, and co-added the resulting cross-correlation functions into a single three-dimensional cross-correlation cube.

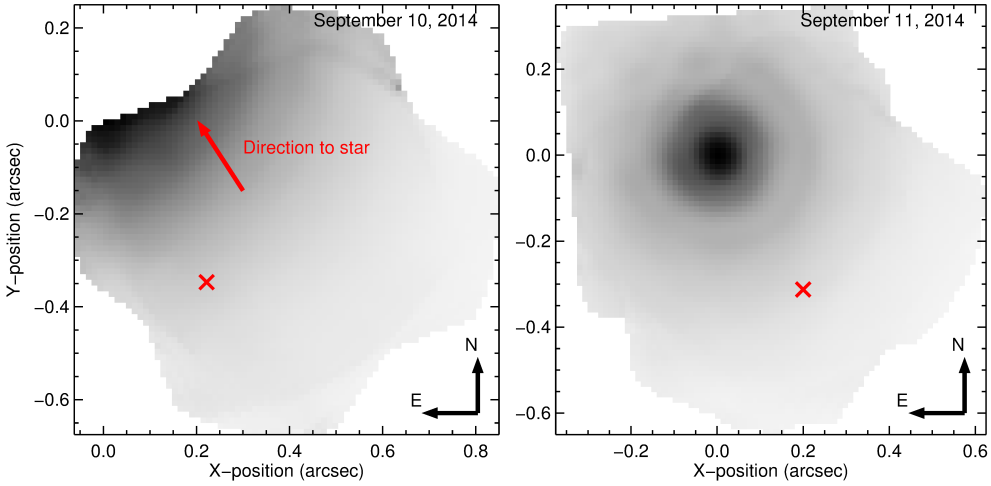

Figure 5.1: Wavelength-averaged images of the β Pictoris SINFONI data, obtained by de-rotating and stacking the exposures of each night, and taking the median flux of the spectrum at each image location. The expected position of β Pictoris b is indicated by the red crosses.

5.4 DATA ANALYSIS

5.4.1 *Removal of starlight*

The flux at each spatial position in the data cube is dominated by the spectrum of the star, showing a few stellar but mainly telluric absorption features. The steps to remove this starlight are shown in Figure 5.3. First, a high signal-to-noise master stellar spectrum is created by combining the spectra from the 1% (20) brightest pixels by first normalizing them to the same flux level and then by taking the mean of these spectra at each wavelength while rejecting $> 6\sigma$ outliers.

For each spatial position in the data cube we subsequently divide the spectrum by this master and apply a Gaussian smoothing filtering with a 1σ width of 10 wavelength steps (~ 300 km s^{-1}). The resulting function is used as a proxy for the local wavelength-dependence of the stellar diffraction pattern. The stellar master spectrum is then multiplied with this proxy and subtracted from the local spectrum. This effectively removes the starlight at each position and wavelength. As a final step, any remaining $> 6\sigma$ outliers are set to zero.

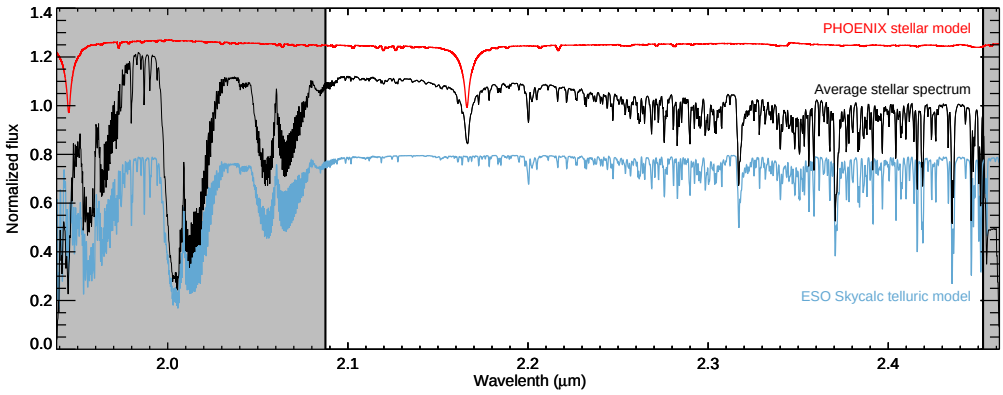

Figure 5.2: The average stellar spectrum of the master cube of the second night (black), compared with a continuum-normalized rotation-broadened PHOENIX model in red (Husser et al., 2013) and the telluric transmission spectrum as obtained using ESO SkyCalc in blue (Noll, S. et al., 2012; Jones, A. et al., 2013), both convolved to the spectral resolution of SINFONI. There are few stellar absorption lines in this wavelength range and the data is dominated by telluric absorption bands due to water, CO_2 and methane. The grey regions at the edges of the waveband were discarded due to strong telluric bands of H_2O and CO_2 or bad pixels that are close to the edges of the detector.

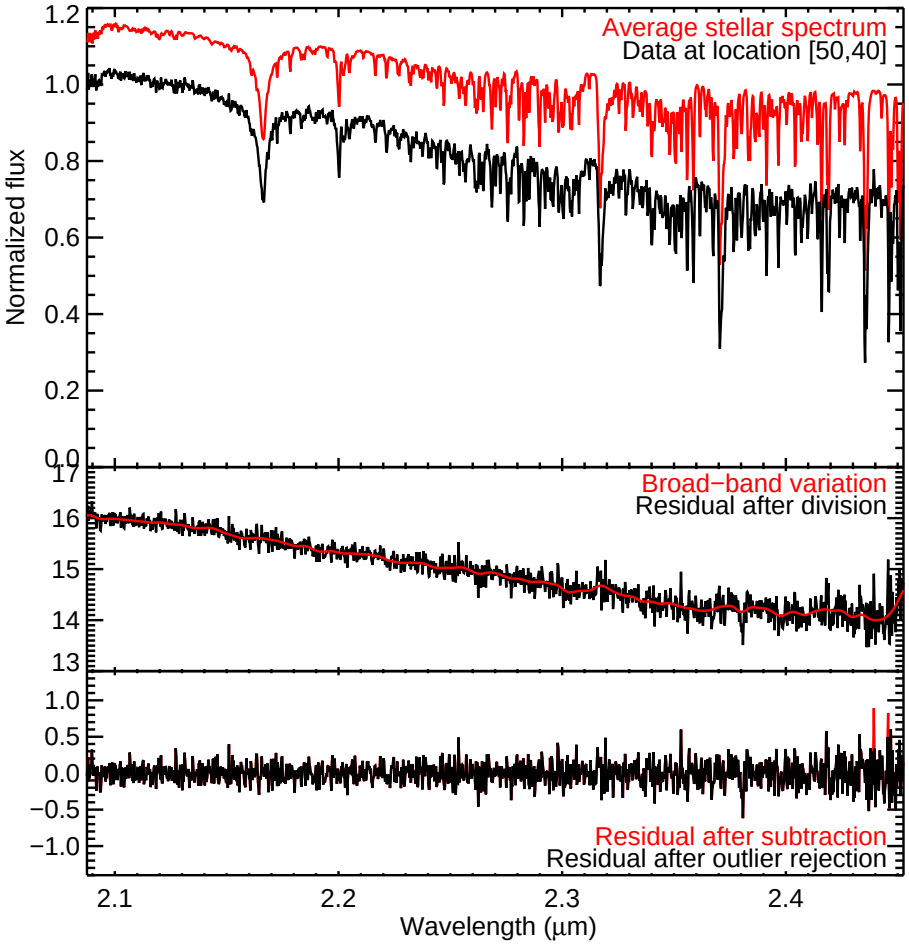

Figure 5.3: Stepwise removal of starlight from each spatial location in the data cubes. **Upper panel:** The master stellar spectrum (red) compared to the local observed spectrum (black) at spatial pixel location [50,40] of the second night. The absolute flux level of the master stellar spectrum is much greater than that at this location, so it is scaled to the level of the local spectrum for visual purposes. **Middle panel:** Ratio of the master spectrum over the local spectrum (black) after application of Gaussian smoothing (red), which is used as a proxy for the local wavelength-dependence of the stellar diffraction pattern. **Bottom panel:** Residuals obtained after subtracting the master stellar spectrum multiplied by the proxy from the local observed spectrum. Pixel values that are more than 6σ away from the mean are rejected (red).

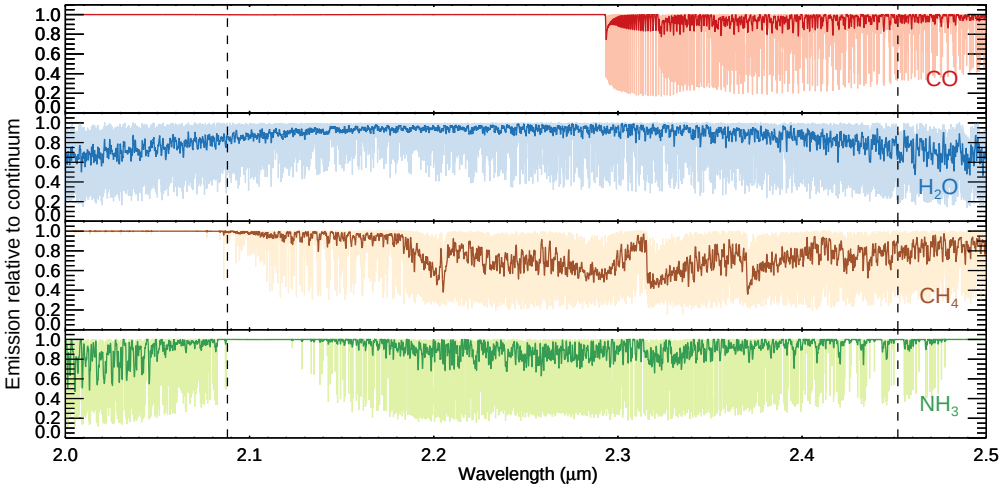

Figure 5.4: Model templates of CO, H_2O, CH_4 and NH_3 at high ($R \sim 10^6$) spectral resolution (light colour) and convolved to a spectral resolution of $R = 5000$ (dark colour). The vertical dashed lines indicate the wavelength range of the data.

5.4.2 *Cross correlation with model templates*

We search for the presence of CO, H_2O, NH_3 and CH_4 at each spatial location in the data cube by cross-correlating each local residual spectrum with a model template of each of these molecules, corresponding to ~ 1200 K emission models of the day side HD 189733, adopted from de Kok et al. (2014). In addition we cross-correlate with a grid of pre-computed BT-Settl model spectra (Allard et al., 2011)[1] with temperatures less than 3000 K and varying in surface gravity from $\log(g) = 2.5$ to 5.5.

Prior to cross-correlation, we fit and subtract the continuum of these model spectra to eliminate low-frequency variations and convolve them to a spectral resolution of $R = 5000$ (see Figure 5.4). These models are then cross-correlated with each residual spectrum over a range of velocities of $v \pm 2500$ km s^{-1} in steps of 10 km s^{-1}. The cross-correlation of the two data cubes therefore results in two cross-correlation cubes with a depth of 501 steps in radial velocity.

At the planet position, the closer the model template matches the real emission spectrum of the planet, the stronger the resulting cross-correlation signal will be. In all other spatial locations no significant cross-correlation signals are expected. The systematic radial velocity of the β Pictoris system is $+20 \pm 0.7$ km s^{-1} (Gontcharov, 2006). Using the orbital solution of Wang

1 https://phoenix.ens-lyon.fr/Grids/BT-Settl/CIFIST2011_2015/FITS/

et al. (2016), we calculate the instantaneous radial velocity of β Pic b to be ~ -9.5 km s^{-1} (the barycentric correction of -7.9 km s^{-1} has been applied by the pipeline). Therefore, the peak cross-correlation is expected to occur at a radial velocity of ~ 10 km s^{-1}, i.e. one velocity step away from zero in our cross-correlation cubes.

5.4.3 *ADI Analysis*

We also analysed the data by means of angular differential imaging using the LOCI algorithm (Lafrenière et al., 2007) to compare the performance of the molecule mapping technique. LOCI was applied independently at each wavelength with a separation criterion of 1 full-width-at-half-maximum, an optimization area of 300 FWHM and a geometry parameter of 0.5.

5.5 RESULTS AND DISCUSSION

5.5.1 *Molecule maps of the β Pictoris system*

The molecule maps at the radial velocity of the planet are shown in Figure 5.5. The maps of CO and H_2O show a significant signal at the expected position of the planet, while the planet is not detected in the maps of NH_3 and CH_4. The one dimensional cross-correlation functions at the position of the planet are shown in Figure 5.6. From these we measure the detection confidence to be 6.9σ and 11.0σ for CO and H_2O respectively, determined from the ratio of the peak to the standard deviation of the cross correlation functions at $|v| > 250$ km s^{-1}.

The non-detections of CH_4 and NH_3 are consistent with the effective temperature of the planet, which at 1724 K is expected to be too high for significant quantities of these particular molecules unless the planet is rich in respectively carbon or nitrogen (Burrows et al., 2006; Hubeny et al., 2007; Zahnle et al., 2014; Heng et al., 2016b; Heng et al., 2016a; Moses et al., 2016; Todorov et al., 2016).

5.5.2 *Cross-correlation with BT-Settl grid*

The BT-Settl model that corresponds most closely to the planet parameters observed by Chilcote et al. (2017), i.e. $T_{\rm eff}$=1700 K and $\log(g)$ =4.0, is used to produce the cross-correlation map shown in the middle panel of Figure 5.7. This model takes into account absorption from both CO and H_2O, and therefore is a more complete representation of the true planet spectrum than the individual molecule spectra. Indeed, the planet is detected at a significantly higher level of 14.4σ. The K-band contrast ratio between β Pic b and

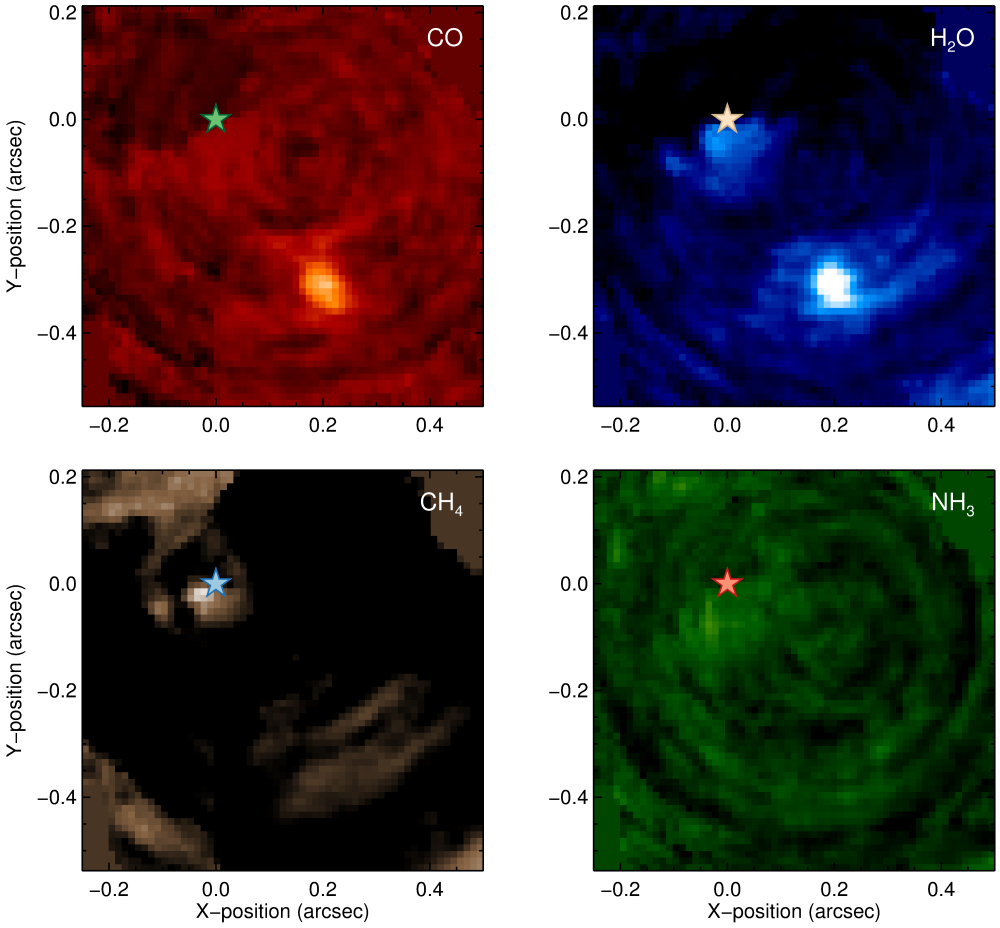

Figure 5.5: Molecule maps of CO, H_2O,CH_4 and NH_3 at $v_{sys} = 10$ km s^{-1}. In all four panels, the colours scale linearly between cross-correlation of -3σ (black) and +8σ (white). The cross-correlation enhancement caused by the planet is detected at a significance of 6.9σ and 11.0σ in the maps of CO and H_2O respectively, but not in CH_4 and NH_3.

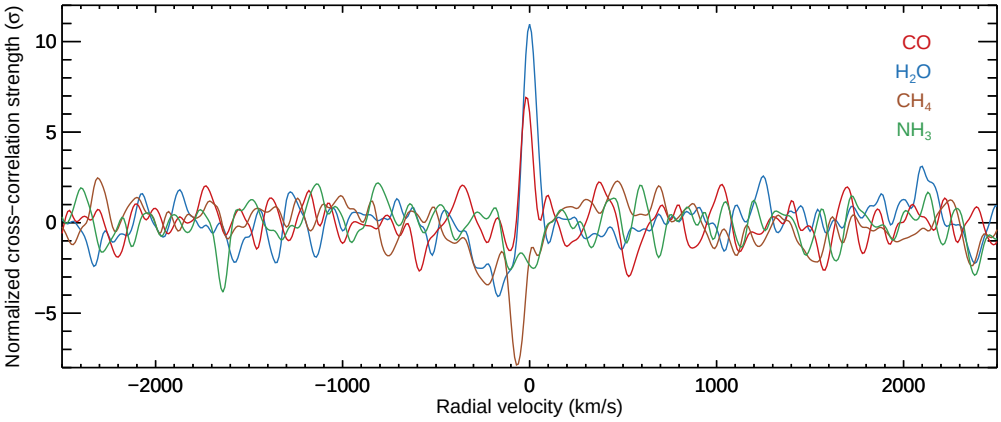

Figure 5.6: 1D cross-correlation functions of CO, H_2O, CH_4 and NH_3 at the location of the planet normalized by their noise level.

its host star is $\Delta K = 9.2 \pm 0.1$ (Bonnefoy et al., 2011). Our 14.4σ detection of the planet therefore corresponds to an achieved 3σ contrast of 4.4×10^{-5}; an improvement of a factor 75 over the raw contrast measured in Section 5.3 (see Figure. 5.8).

The left panel of Figure 5.7 shows the white-light image obtained with the LOCI algorithm for which these observations were initially intended. Although there is a clear peak at the planet position, it is difficult to assess the statistical confidence of this detection. Several other positive and negative features with similar amplitudes as that of the signal at the planet position are present in the image, in particular close to the host star.

Global atmospheric parameters such as the effective temperature, surface gravity, metallicity and abundances ratios, influence the relative strength of individual absorption lines. These may significantly influence the cross-correlation function thus making the analysis sensitive to underlying model parameters. Figure 5.9 shows the peak value of the 1D cross-correlation function with BT-Settl models with varying T_{eff} and $\log(g)$. The cross-correlation peak steeply decreases for temperatures below $\sim$ 1600 K because the strength of the water absorption features at > 2.1 µm become significantly weaker.

Above $\sim$ 2000 K, the cross-correlation peak is a shallower function of T_{eff} as the CO and H_2O absorption bands slowly diminish towards higher temperatures. Similarly, models with $\log(g)$ below 5.0 are favoured over models with higher surface gravities, due to the stronger water absorption bands relative to CO for lower values of $\log(g)$. The highest cross-correlation peak is achieved for $T_{eff} = 1700$ K and $\log(g) = 3.5$, with a signal-to-noise of 14.4σ (see Figure 5.7). Although preliminary, this analysis shows that medium resolution integral-field spectrographs can be used to characterize the funda-

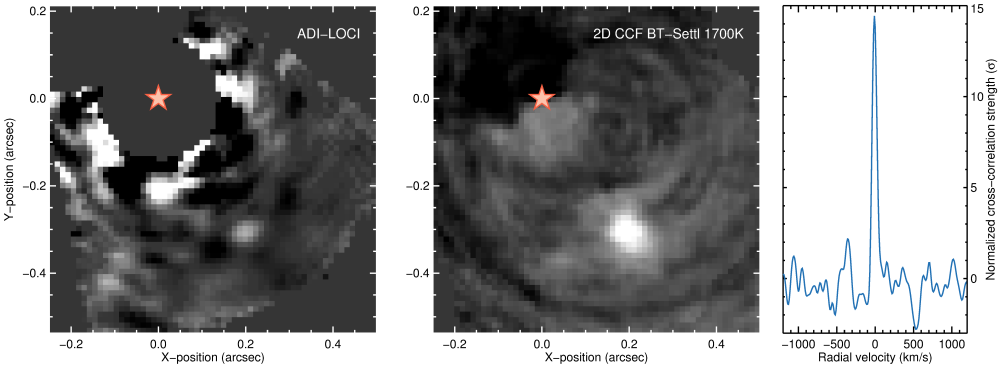

Figure 5.7: **Left panel:** White-light image obtained after co-adding the data with the LOCI algorithm. The planet is visible near [0.2",-0.3"], but is barely recovered. **Middle panel:** Cross-correlation map using the preferred BT-Settl model (T_{eff} = 1700 K and log(g) = 3.5). The grey scales are set between −3 and +14σ. **Right panel:** The one-dimensional cross-correlation function at the location of the planet. The BT-Settl model cross-correlates with the planet at a confidence of 14.4σ.

mental parameters of directly imaged companions via cross-correlation, and that molecule mapping is not limited to only the detection of molecules in the atmospheres of these objects.

5.5.3 *Residual structure in the molecule maps*

The cross-correlation map of CH_4, and to a lesser extent that of H_2O, show systematic correlation signals throughout the image. This is caused by residual telluric absorption that was incompletely or too strongly corrected by our cleaning procedure – most importantly the strong telluric CH_4 feature at 2.32 μm that dominates the absorption spectra of both hot and cold CH_4 gas. This is the result of a mismatch between the local spectra and the stellar master spectrum used to remove the starlight and notably occurs near the edges of individual frames and at the location of the star, where the signal-to-noise of the residuals is high.

We suspect that the systematic correlation signals are caused by stray light in the instrument that was not corrected by the data reduction pipeline. Such spurious light dilutes the spectra and thereby changes the relative depth of spectral lines. Because there is no one-to-one correspondence between the position of a spectrum on the CCD and the location in the image, stray light results in irregular cross-correlation patterns as can be seen in the data. A careful treatment of stray light during the data reduction may partly mitigate this problem. However, the spatial structure of the systematic correlation sig-

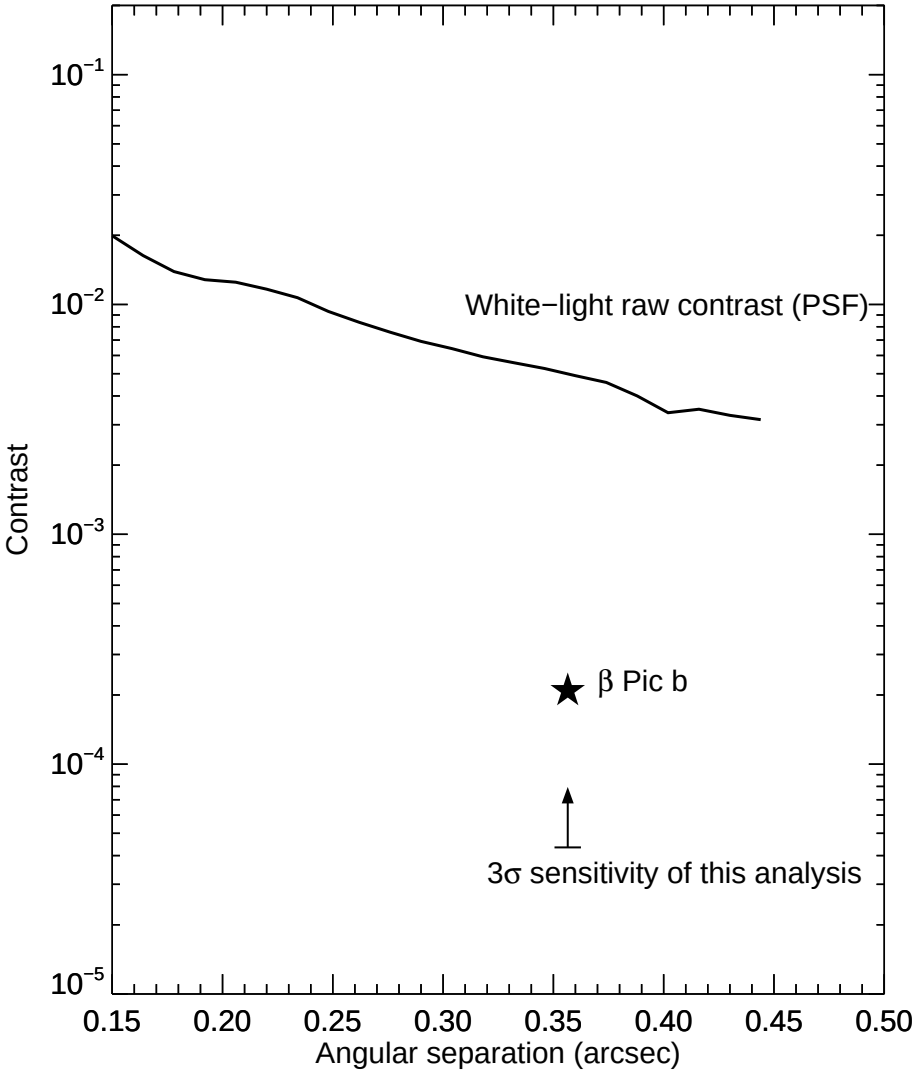

Figure 5.8: Raw-contrast curve obtained by averaging the flux from the second night in annuli with widths of 20 mas around the central star, normalized by the peak flux. The actual K-band contrast of β Pic b is adopted from Bonnefoy et al. (2011) and the 3σ sensitivity limit of this analysis is derived from our 14.4σ detection of the planet.

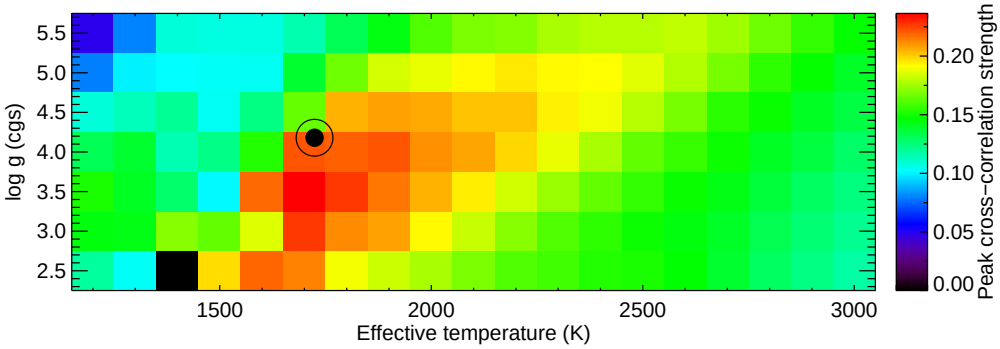

Figure 5.9: The planet cross-correlation peak as a function of BT-Settl models with varying T_{eff} and $\log(g)$. The cross-correlation peak steeply decreases for temperatures below ~ 1600 K because the strength of the water absorption features at > 2.1 μm become significantly weaker. All molecular bands diminish above temperatures of ~ 2000 K, causing a slow decrease of the cross-correlation function at higher temperatures. The black circle corresponds to the values reported by Chilcote et al. (2017).

nals is clearly not point-like and is therefore not readily confused with that of a planet.

5.5.4 *Molecule mapping from space with NIRSpec and MIRI*

Molecule mapping provides new possibilities for high-contrast imaging using R ~ 5000 IFSs, also on instruments aboard space-based observatories. Both NIRSpec and MIRI on the James Webb Space Telescope (JWST), to be launched in 2018, have integral-field capabilities. In IFS mode, NIRSpec covers wavelengths from 0.7 and 5.27 μm at a spectral resolution of ~ 2.700 with a spatial sampling of 0.1" × 0.1". MIRI has a similar IFS mode, operating between 4.89 μm to 28.45 μm at a spectral resolution varying from 3320 at short wavelengths to 1460 at longer wavelengths. The waveband is divided into four channels with increasing slit-size, the bluest channel having a spatial resolution of 0.196", and the reddest a spatial resolution of 0.276". Although the spatial sampling of both NIRSpec and MIRI is significantly more coarse than that of SINFONI in 25 mas plate-scale mode, objects with a separation down to 0.1" can theoretically be resolved by the IFS of NIRSpec, and separations down to 0.2" can be resolved by MIRI at 5 μm .

5.5.5 *Molecule mapping with HARMONI at the ELT*

The primary spectroscopic capability of the ELT in the near infra-red will be fulfilled by the HARMONI integral-field spectrograph. HARMONI will cover wavelengths between 0.47 to 2.45 μm at spectral resolutions ranging from $R \sim 400$ to $\sim 20,000$ in individual Z, J, H and K bands. The highest possible spatial sampling is 4 mas, equivalent to the diffraction limit of the ELT (Thatte et al., 2014).

To first order, the signal-to-noise achieved by cross-correlation scales with the signal-to-noise per wavelength element of the planet's absorption lines times the square root of the number of lines in the waveband (Snellen et al., 2015). For bright stars at near-infrared wavelengths, we can assume that the noise is dominated by the photon noise of the stellar PSF, which scales with the mirror diameter D. The signal-to-noise of the planet spectral lines scales with the square root of the spectral resolving power, so the signal to noise of HARMONI compared to SINFONI can be approximated as:

$$\frac{S/N_{HARMONI}}{S/N_{SINFONI}} = \frac{D_{ELT}\sqrt{R_{HARMONI}}}{D_{VLT}\sqrt{R_{SINFONI}}} = 9.75$$

assuming the maximum spectral resolution of HARMONI, but otherwise equal wavelength coverage and instrument throughput. This indicates that HARMONI can achieve the same sensitivity as SINFONI in $\sim 1\%$ of the exposure time, but for planets that are five times closer to their host star because the diffraction pattern scales with the inverse of the mirror diameter.

With a spectral resolving power of 20,000, the systemic and orbital velocities of target planets can be resolved by the cross-correlation function. In addition to discovering a companion and spectrally characterizing its atmosphere, the HARMONI instrument can therefore be used to establish co-movement with the host star and constrain its orbit via the instantaneous radial velocity. We conceive that this can be achieved in a single observation, making HARMONI especially suitable for the characterization of young giant exoplanets.

5.6 CONCLUSION

This study introduces the first application of the molecule mapping technique for detecting close-in substellar companions using AO-assisted medium-resolution integral field spectroscopy. With molecule mapping, integral-field spectra are cross-correlated with molecular template spectra to search for the spectral signatures of spatially resolved exoplanets that are embedded in the photon noise of the dominating star light. The cross-correlation co-adds the individual absorption lines of the planet spectrum at the spatial location of the planet, while this is not the case for (residual) telluric and stellar features.

We applied molecule mapping to 2.5 hours of archival SINFONI observations of the β Pictoris system. By cross-correlating the integal-field data cubes with templates of CO, H_2O, CH_4 and NH_3, we obtained 6.9σ and 11.0σ detections of CO and H_2O in the atmosphere of the planet. We also cross-correlated with a grid of BT-Settl models, varying the effective temperature between 1200 K − 3000 K, and the surface gravity between $\log(g) = 2.5 - 5.5$. We found that the cross-correlation peaks for $T_{\rm eff} = 1700$ K and $\log(g) = 3.5$, and show that molecule mapping can therefore constrain the fundamental parameters of young gas giant planets. With these model parameters, the planet was detected at a confidence of 14.4σ, corresponding to a 3σ contrast of 4.4×10^{-5}. We also analysed the same data using the LOCI algorithm. In this case the planet was only marginally detected. This result demonstrates molecule mapping can significantly enhance the sensitivity of IFS observations at medium spectral resolution over established direct imaging techniques.

Our successful application of molecule mapping on existing SINFONI data feeds expectations for the potential of upcoming medium-resolution integral-field instruments on the JWST and the ELT. We briefly outlined the specifications of MIRI and NIRSpec (JWST) and HARMONI (ELT) and anticipate that these instruments will benefit significantly from cross-correlation based analyses. We therefore strongly advocate observations of young giant exoplanets with MIRI, NIRSpec and HARMONI.

ACKNOWLEDGEMENTS

This work is part of research programme VICI 639.043.107, funded by the Dutch Organisation for Scientific Research (NWO). Snellen acknowledges funding from the European Research Council (ERC) under the European Union's Horizon 2020 research and innovation programme under grant agreement No 694513. This work is based on observations collected at the European Organisation for Astronomical Research in the Southern Hemisphere under ESO programme 093.C-0626(A).

BIBLIOGRAPHY

Allard, F., D. Homeier, and B. Freytag (2011). „Model Atmospheres From Very Low Mass Stars to Brown Dwarfs." In: *16th Cambridge Workshop on Cool Stars, Stellar Systems, and the Sun*. Ed. by C. Johns-Krull, M. K. Browning, and A. A. West. Vol. 448. Astronomical Society of the Pacific Conference Series, p. 91. arXiv: 1011.5405 [astro-ph.SR].

Augereau, J. C. et al. (2001). „Dynamical modeling of large scale asymmetries in the beta Pictoris dust disk." In: *A&A* 370, pp. 447–455. DOI: 10.1051/0004-6361:20010199. eprint: astro-ph/0102069.

Baraffe, I. et al. (2003). „Evolutionary models for cool brown dwarfs and extrasolar giant planets. The case of HD 209458." In: *A&A* 402, pp. 701–712. DOI: 10.1051/0004-6361:20030252. eprint: astro-ph/0302293.

Barman, T. S. et al. (2015). „Simultaneous Detection of Water, Methane, and Carbon Monoxide in the Atmosphere of Exoplanet HR8799b." In: *ApJ* 804, 61, p. 61. DOI: 10.1088/0004-637X/804/1/61. arXiv: 1503.03539 [astro-ph.EP].

Bell, C. P. M., E. E. Mamajek, and T. Naylor (2015). „A self-consistent, absolute isochronal age scale for young moving groups in the solar neighbourhood." In: *MNRAS* 454, pp. 593–614. DOI: 10.1093/mnras/stv1981. arXiv: 1508.05955 [astro-ph.SR].

Beuzit, J.-L. et al. (2008). „SPHERE: a 'Planet Finder' instrument for the VLT." In: *Ground-based and Airborne Instrumentation for Astronomy II*. Vol. 7014. Proc. SPIE, p. 701418. DOI: 10.1117/12.790120.

Bonnefoy, M. et al. (2011). „High angular resolution detection of β Pictoris b at 2.18 μm." In: *A&A* 528, L15, p. L15. DOI: 10.1051/0004-6361/201016224.

Bowler, B. P. (2016). „Imaging Extrasolar Giant Planets." In: *PASP* 128.10, p. 102001. DOI: 10.1088/1538-3873/128/968/102001. arXiv: 1605.02731 [astro-ph.EP].

Burrows, A., D. Sudarsky, and I. Hubeny (2006). „L and T Dwarf Models and the L to T Transition." In: *ApJ* 640, pp. 1063–1077. DOI: 10.1086/500293. eprint: astro-ph/0509066.

Burrows, C. J. et al. (1995). „HST Observations of the Beta Pictoris Circumstellar Disk." In: *American Astronomical Society Meeting Abstracts*. Vol. 27. Bulletin of the American Astronomical Society, p. 1329.

Chauvin, G. (2016). „Direct Imaging of Exoplanets Living an Exciting Life." In: *Young Stars & Planets Near the Sun*. Ed. by J. H. Kastner, B. Stelzer, and S. A. Metchev. Vol. 314. IAU Symposium, pp. 213–219. DOI: 10.1017/S1743921315006560.

Chilcote, J. et al. (2017). „1-2.4 μm Near-IR Spectrum of the Giant Planet β Pictoris b Obtained with the Gemini Planet Imager." In: *AJ* 153, 182, p. 182. DOI: 10.3847/1538-3881/aa63e9. arXiv: 1703.00011 [astro-ph.EP].

Currie, T. et al. (2017). „Subaru/SCExAO First-light Direct Imaging of a Young Debris Disk around HD 36546." In: *ApJ* 836, L15, p. L15. DOI: 10.3847/2041-8213/836/1/L15. arXiv: 1701.02314 [astro-ph.EP].

de Kok, R. J. et al. (2014). „Identifying new opportunities for exoplanet characterisation at high spectral resolution." In: *A&A* 561, A150, A150. DOI: 10.1051/0004-6361/201322947. arXiv: 1312.3745 [astro-ph.EP].

Ducati, J. R. (2002). „VizieR Online Data Catalog: Catalogue of Stellar Photometry in Johnson's 11-color system." In: *VizieR Online Data Catalog* 2237.

Eisenhauer, F. et al. (2003). „SINFONI - Integral field spectroscopy at 50 milliarcsecond resolution with the ESO VLT." In: *Instrument Design and Performance for Optical/Infrared Ground-based Telescopes*. Ed. by M. Iye and A. F. M. Moorwood. Vol. 4841. Proc. SPIE, pp. 1548–1561. DOI: 10.1117/12.459468. eprint: astro-ph/0306191.

Fitzgerald, M. P. and J. R. Graham (2006). „Speckle Statistics in Adaptively Corrected Images." In: *ApJ* 637, pp. 541–547. DOI: 10.1086/498339. eprint: astro-ph/0510503.

Gontcharov, G. A. (2006). „Pulkovo Compilation of Radial Velocities for 35495 Hipparcos stars in a common system." In: *Astronomy Letters* 32, pp. 759–771. DOI: 10.1134/S1063773706110065. arXiv: 1606.08053 [astro-ph.SR].

Gray, R. O. et al. (2006). „Contributions to the Nearby Stars (NStars) Project: Spectroscopy of Stars Earlier than Mo within 40 pc-The Southern Sample." In: *AJ* 132, pp. 161–170. DOI: 10.1086/504637. eprint: astro-ph/0603770.

Guyon, O. (2011). „High performance coronagraphy for direct imaging of exoplanets." In: *European Physical Journal Web of Conferences*. Vol. 16. European Physical Journal Web of Conferences, p. 03001. DOI: 10.1051/epjconf/20111603001.

Heng, K. and J. R. Lyons (2016a). „Carbon Dioxide in Exoplanetary Atmospheres: Rarely Dominant Compared to Carbon Monoxide and Water in Hot, Hydrogen-dominated Atmospheres." In: *ApJ* 817, 149, p. 149. DOI: 10.3847/0004-637X/817/2/149. arXiv: 1507.01944 [astro-ph.EP].

Heng, K. and S.-M. Tsai (2016b). „Analytical Models of Exoplanetary Atmospheres. III. Gaseous C-H-O-N Chemistry with Nine Molecules." In: *ApJ* 829, 104, p. 104. DOI: 10.3847/0004-637X/829/2/104. arXiv: 1603.05418 [astro-ph.EP].

Hubeny, I. and A. Burrows (2007). „A Systematic Study of Departures from Chemical Equilibrium in the Atmospheres of Substellar Mass Objects." In: *ApJ* 669, pp. 1248–1261. DOI: 10.1086/522107. arXiv: 0705.3922.

Husser, T.-O. et al. (2013). „A new extensive library of PHOENIX stellar atmospheres and synthetic spectra." In: *A&A* 553, A6, A6. DOI: 10.1051/0004-6361/201219058. arXiv: 1303.5632 [astro-ph.SR].

Jones, A. et al. (2013). „An advanced scattered moonlight model for Cerro Paranal." In: *A&A* 560, A91. DOI: 10.1051/0004-6361/201322433. URL: http://dx.doi.org/10.1051/0004-6361/201322433.

Jovanovic, N. et al. (2015). „The Subaru Coronagraphic Extreme Adaptive Optics System: Enabling High-Contrast Imaging on Solar-System Scales." In: *PASP* 127, p. 890. DOI: 10.1086/682989. arXiv: 1507.00017 [astro-ph.IM].

Kawahara, H. et al. (2014). „Spectroscopic Coronagraphy for Planetary Radial Velocimetry of Exoplanets." In: *ApJ* 212, 27, p. 27. DOI: 10.1088/0067-0049/212/2/27. arXiv: 1404.5712 [astro-ph.EP].

Kenworthy, M. (2017). „Looking for rings and things." In: *Nature Astronomy* 1, 0099, p. 0099. DOI: 10.1038/s41550-017-0099.

Konopacky, Q. M. et al. (2013). „Detection of Carbon Monoxide and Water Absorption Lines in an Exoplanet Atmosphere." In: *Science* 339, pp. 1398–1401. DOI: 10.1126/science.1232003. arXiv: 1303.3280 [astro-ph.EP].

Lafrenière, D. et al. (2007). „A New Algorithm for Point-Spread Function Subtraction in High-Contrast Imaging: A Demonstration with Angular Differential Imaging." In: *ApJ* 660, pp. 770–780. DOI: 10.1086/513180. eprint: astro-ph/0702697.

Lagrange, A.-M. et al. (2009). „A probable giant planet imaged in the β Pictoris disk. VLT/NaCo deep L'-band imaging." In: *A&A* 493, pp. L21–L25. DOI: 10.1051/0004-6361:200811325. arXiv: 0811.3583.

Lagrange, A.-M. et al. (2010). „A Giant Planet Imaged in the Disk of the Young Star β Pictoris." In: *Science* 329, p. 57. DOI: 10.1126/science.1187187. arXiv: 1006.3314 [astro-ph.EP].

Lazzaro, D. et al. (1994). „Is there a planet around beta Pictoris? Perturbations of a planet circumstellar dust disk. 2: The analytical model." In: *Icarus* 108, pp. 59–80. DOI: 10.1006/icar.1994.1041.

Lecavelier des Etangs, A. and A. Vidal-Madjar (2016). „The orbit of beta Pictoris b as a transiting planet." In: *A&A* 588, A60, A60. DOI: 10.1051/0004-6361/201527631. arXiv: 1602.04683 [astro-ph.EP].

Lecavelier des Etangs, A. et al. (1996). „Perturbations of a Planet on the β Pictoris Circumstellar Dust Disk. 3. Time Scale of Collisional Destruction versus Resonance Time Scale." In: *Icarus* 123, pp. 168–179. DOI: 10.1006/icar.1996.0147.

Luger, R. et al. (2017). „The Pale Green Dot: A Method to Characterize Proxima Centauri b Using Exo-Aurorae." In: *ApJ* 837, 63, p. 63. DOI: 10.3847/1538-4357/aa6040. arXiv: 1609.09075 [astro-ph.EP].

Macintosh, B. et al. (2006). „The Gemini Planet Imager." In: *Society of Photo-Optical Instrumentation Engineers (SPIE) Conference Series*. Vol. 6272. Proc. SPIE, p. 62720L. DOI: 10.1117/12.672430.

Macintosh, B. et al. (2014). „First light of the Gemini Planet Imager." In: *Proceedings of the National Academy of Science* 111, pp. 12661–12666. DOI: 10.1073/pnas.1304215111. arXiv: 1403.7520 [astro-ph.EP].

Marois, C. et al. (2008). „Direct Imaging of Multiple Planets Orbiting the Star HR 8799." In: *Science* 322, p. 1348. DOI: 10.1126/science.1166585. arXiv: 0811.2606.

Mawet, D. et al. (2012). „Review of small-angle coronagraphic techniques in the wake of ground-based second-generation adaptive optics systems." In: *Space Telescopes and Instrumentation 2012: Optical, Infrared, and Millimeter Wave*. Vol. 8442. Proc. SPIE, p. 844204. DOI: 10.1117/12.927245. arXiv: 1207.5481 [astro-ph.IM].

Mesa, D. et al. (2017). „Upper limits for mass and radius of objects around Proxima Cen from SPHERE/VLT." In: *MNRAS* 466, pp. L118–L122. DOI: 10.1093/mnrasl/slw241. arXiv: 1611.10362 [astro-ph.EP].

Moses, J. I. et al. (2016). „On the Composition of Young, Directly Imaged Giant Planets." In: *ApJ* 829, 66, p. 66. DOI: 10.3847/0004-637X/829/2/66. arXiv: 1608.08643 [astro-ph.EP].

Mouillet, D. et al. (1997). „A planet on an inclined orbit as an explanation of the warp in the Beta Pictoris disc." In: *MNRAS* 292, p. 896. DOI: 10.1093/mnras/292.4.896. eprint: astro-ph/9705100.

Noll, S. et al. (2012). „An atmospheric radiation model for Cerro Paranal." In: *A&A* 543, A92. DOI: 10.1051/0004-6361/201219040. URL: http://dx.doi.org/10.1051/0004-6361/201219040.

Rameau, J. et al. (2015). „Detection limits with spectral differential imaging data." In: *A&A* 581, A80, A80. DOI: 10.1051/0004-6361/201525879.

Riaud, P. and J. Schneider (2007). „Improving Earth-like planets' detection with an ELT: the differential radial velocity experiment." In: *A&A* 469, pp. 355–361. DOI: 10.1051/0004-6361:20077085.

Roques, F. et al. (1994). „Is there a planet around beta Pictoris? Perturbations of a planet on a circumstellar dust disk. 1: The numerical model." In: *Icarus* 108, pp. 37–58. DOI: 10.1006/icar.1994.1040.

Royer, F., J. Zorec, and A. E. Gómez (2007). „Rotational velocities of A-type stars. III. Velocity distributions." In: *A&A* 463, pp. 671–682. DOI: 10.1051/0004-6361:20065224. eprint: astro-ph/0610785.

Ruffio, J.-B. et al. (2017). „Improving and Assessing Planet Sensitivity of the GPI Exoplanet Survey with a Forward Model Matched Filter." In: *ApJ* 842, 14, p. 14. DOI: 10.3847/1538-4357/aa72dd. arXiv: 1705.05477 [astro-ph.EP].

Scholl, H., F. Roques, and B. Sicardy (1993). „Resonance trapping of circumstellar dust particles by an alleged planet." In: *Celestial Mechanics and Dynamical Astronomy* 56, pp. 381–393. DOI: 10.1007/BF00699748.

Smith, Bradford A. and Richard J. Terrile (1984). „A Circumstellar Disk Around β Pictoris." In: *Science* 226.4681, pp. 1421–1424. ISSN: 0036-8075. DOI: 10.

1126/science.226.4681.1421. eprint: http://science.sciencemag.org/content/226/4681/1421.full.pdf. URL: http://science.sciencemag.org/content/226/4681/1421.

Snellen, I. A. G. et al. (2014). „Fast spin of the young extrasolar planet β Pictoris b." In: *Nature* 509, pp. 63–65. DOI: 10.1038/nature13253.

Snellen, I. et al. (2015). „Combining high-dispersion spectroscopy with high contrast imaging: Probing rocky planets around our nearest neighbors." In: *A&A* 576, A59, A59. DOI: 10.1051/0004-6361/201425018. arXiv: 1503.01136 [astro-ph.EP].

Sparks, W. B. and H. C. Ford (2002). „Imaging Spectroscopy for Extrasolar Planet Detection." In: *ApJ* 578, pp. 543–564. DOI: 10.1086/342401. eprint: astro-ph/0209078.

Thatte, N. A. et al. (2014). „HARMONI: the first light integral field spectrograph for the E-ELT." In: *Ground-based and Airborne Instrumentation for Astronomy V*. Vol. 9147. Proc. SPIE, p. 914725. DOI: 10.1117/12.2055436.

Todorov, K. O. et al. (2016). „The Water Abundance of the Directly Imaged Substellar Companion κ And b Retrieved from a Near Infrared Spectrum." In: *ApJ* 823, 14, p. 14. DOI: 10.3847/0004-637X/823/1/14. arXiv: 1504.00217 [astro-ph.EP].

van Leeuwen, F. (2007). „Validation of the new Hipparcos reduction." In: *A&A* 474, pp. 653–664. DOI: 10.1051/0004-6361:20078357. arXiv: 0708.1752.

Wang, J. J. et al. (2016). „The Orbit and Transit Prospects for β Pictoris b Constrained with One Milliarcsecond Astrometry." In: *AJ* 152, 97, p. 97. DOI: 10.3847/0004-6256/152/4/97. arXiv: 1607.05272 [astro-ph.EP].

Wang, J. et al. (2017). „Observing Exoplanets with High Dispersion Coronagraphy. I. The Scientific Potential of Current and Next-generation Large Ground and Space Telescopes." In: *AJ* 153, 183, p. 183. DOI: 10.3847/1538-3881/aa6474. arXiv: 1703.00582 [astro-ph.EP].

Zahnle, K. J. and M. S. Marley (2014). „Methane, Carbon Monoxide, and Ammonia in Brown Dwarfs and Self-Luminous Giant Planets." In: *ApJ* 797, 41, p. 41. DOI: 10.1088/0004-637X/797/1/41. arXiv: 1408.6283 [astro-ph.EP].